Time-dependent optical phase and imaginary collision kernels

J. E. Thomas, P. J. Laverty, and K. D. Stokes

Department of Physics, Duke University, Durham, North Carolina 27706

(Received 16 February 1989)

Recently demonstrated techniques for measuring collision-induced *phase* in macroscopic optical coherence are described and analyzed in detail. The time-dependent phase measured by this method is used to study *imaginary* collision kernels for optical radiators that are related to the phase by Fourier transformation. The results indicate that classical velocity changes may make an important contribution to the imaginary kernel, in contrast to the real kernel, which is dominated by diffractive velocity changes.

I. INTRODUCTION

Since the early 1970s, it has been appreciated that a complete description of velocity-changing collisions for optical radiators (optical coherence) in vapors requires a quantum-mechanical treatment for both the internal and center-of-mass degrees of freedom.[1-3] This is due to the fact that an optical radiator consists of a superposition of ground and excited electronic states, each of which is shifted and deflected differently in a collision with a perturber. In collision experiments that study the motion of optical radiators, only the oscillating part of the atomic charge distribution is observed in the measurement. The differential-scattering cross section then is determined by the overlap of the quantum-mechanical scattering amplitudes for the superposed states. When the collision potentials for the superposed states are not identical, the differential-scattering cross section will not be real. Physically, this is due to the phase change acquired by the radiator during a collision. As a consequence, the corresponding collision-induced velocity change distribution (i.e., the velocity-changing kernel) and the total-collision cross section will have both a *real* and an *imaginary* component.[4]

Considerable information on the real part of the velocity-changing kernel for infrared and optical radiators has been obtained by measuring the time-dependent decay of the intensity of two-pulse photon echoes. The long measurement time scales obtainable with photon-echo techniques yield correspondingly high-velocity resolution. Radiator destruction and velocity-changing cross sections, and average velocity changes per collision, have been measured by this technique for infrared[5,6] and optical radiators.[7,8] It has been demonstrated that the real part of the velocity-changing kernel for an optical radiator is principally diffractive, the measured velocity changes exhibiting perturber mass, total-cross-section scaling, and magnitude characteristic of diffraction.[8]

Imaginary kernels, by contrast, appear to be relatively unexplored, although they are a unique feature of the scattering of superpositions of dissimilar states. Unlike the real kernel, for which long-range interactions with small phase shifts make important contributions, the imaginary kernel requires for its existence nonzero phase

shifts. It is therefore particularly well suited to investigating large phase-shift effects such as the "trajectory separation,"[4] which arises when the classical paths for the superposed states do not coincide. This occurs for impact parameters below the Weisskopf radius, where the relative phase shift of the superposed states is of order 1 rad. It has been shown that, in this case, the classical collision trajectories are separated in direction by more than a diffraction angle, which is the uncertainty in the classical scattering angle.[4] Prior to the work presented here, only indirect information on imaginary kernels has been obtained from the nonlinear pressure dependence of the line shift measured for infrared radiators.[9]

In this paper we describe in detail new techniques that measure time-dependent optical *phase* in vapors to study *imaginary* collision kernels for optical coherence.[10,11] An important feature of the work is the creation of optical Ramsey fringes in the velocity distribution of the population inversion. These are generated by means of two optical pump pulses and lead to a fringelike absorption profile for a weak counterpropagating probe beam. Collision-induced phase is readily determined by comparing the probe absorption fringes obtained simultaneously in two vapor cells, one with perturbing gas, the other without. The results of the measurements indicate that classical velocity changes may make an important contribution to the imaginary part of the velocity-changing kernel in contrast to the real part, which is dominated by diffractive velocity changes.

Optical Ramsey fringes have been investigated previously for improving spectral resolution in both vapors and beams,[12] but application to collision-induced optical phase measurement was not explored. Recently, velocity-changing collisions of ground-state Zeeman coherence in Sm vapor has been investigated using collision-induced Ramsey resonances.[13] In this work, sublevel coherence is created in a selected velocity group using a modulated pump laser. Velocity-changing collisions transport this coherence to another velocity group which interacts with a probe field tuned to resonate on a coupled transition. This leads to a radiated field at a frequency equal to that of the probe plus or minus the Zeeman shift. The phase of the field is determined by the difference between the pump modulation frequency and

the Zeeman shift and the time needed for the coherence to diffuse between the selected velocity groups. This leads to a Ramsey fringe in the signal observed using Raman heterodyne detection.[13] Although the technique is in principle sensitive to the collision-induced phase of the Zeeman coherence, only the diffusion-time distributions were measured in the experiments.

This paper is organized as follows. Section II presents the basic experimental technique and summarizes the results of detailed calculations which are presented in the Appendix. Section III describes the Fourier-transform technique, which is employed to obtain the raw phases from the data. Results and conclusions are summarized in Secs. IV and V.

II. EXPERIMENTAL TECHNIQUE

An important feature of the technique presented in this paper is the use of velocity-space Ramsey fringes to measure collision-induced optical *phase* in vapors. This method, which is quite easy to implement, is depicted in Fig. 1. The experiments are performed in ^{174}Yb utilizing the $^1S_0 \rightarrow {}^3P_1$ transition at 556 nm. In this case, the nuclear spin is zero, and the system behaves as an ideal two-level medium (i.e., a $J = 0 \rightarrow 1$ transition).[8] Two optical pulses (~ 10 mW/mm^2) separated by a time delay T are generated by acousto-optic modulation of stable c.w. dye-laser radiation[8] and propagate into a heated vapor cell containing Yb and a rare-gas perturber. This produces a Ramsey-fringe-like population inversion in the Yb as a function of velocity due to the Doppler shift of the moving atoms (i.e., the time-separated pulses produce frequency-space fringes).

Neglecting for the moment the effects of collisions, the appearance of a fringelike inversion can be understood physically, as follows. Just after the first input pulse, a macroscopic polarization is created in the medium, where each atom radiates at the natural frequency ω_0 in its rest

frame. The power absorbed by a given group of atoms from the second pulse depends on the relative phase between the polarization and the field of the second pulse at time T. For atoms moving at speed v along the pulse propagation direction, this phase is the product of the frequency detuning as seen by the moving atoms and the time delay T. This is just $\phi = (\omega + \omega_{AO} - kv - \omega_0)T$ in the absence of collisions, where k is the optical wave vector $2\pi/\lambda$, ω_{AO} is the frequency shift of the acousto-optic modulator, and ω the unshifted laser frequency. For pulses of zero duration, the inversion will be $\propto \cos\phi$. Hence, due to the Doppler shift kv, a population inversion with fringelike velocity dependence is created in the medium.

In the experiments, the absorption α of a weak counterpropagating c.w. probe wave (~ 0.2 μW) originating from the same laser is measured as a function of laser frequency ω. For a fixed-input pulse separation T, this measurement is performed at a fixed time just after $2T$ relative to the first input pulse. The reason for making the measurements at time $2T$ when the input pulses separated by a time T will be explained below. The absorption of the weak probe wave depends on the population inversion of the velocity group v, which is resonant with the probe. This requires $\omega + kv = \omega_0$. Solving for v and inserting in the time-dependent phase ϕ yields $\phi = 2\Delta T$, where $\Delta \equiv \omega - \omega_0 + \omega_{AO}/2$. Hence, the probe absorption versus laser frequency contains a fringelike component $\propto \cos(2\Delta T)$.

In the presence of velocity-changing collisions of the optical polarization, the phase $\phi = 2\Delta T$ of the absorption fringe measured at time $2T$ is altered by a time-dependent phase $\varphi(2T)$. The probe absorption fringe is then $\propto \cos(2\Delta T + \varphi)$.

For *finite* duration pulses, the fringelike part of the absorption signal takes the general form

$$\alpha(\Delta) = A_c(\Delta)\cos(2\Delta T + \varphi) + A_s(\Delta)\sin(2\Delta T + \varphi), \quad (1)$$

where the sine term arises because the finite-duration pulses lead to a finite range of effective pulse separations. Collision-induced phase $\varphi(2T)$ is determined by comparing simultaneous absorption traces from cells at different perturber pressure as a function of Δ, Fig. 2. As discussed in Sec. III, fast Fourier transformation is used to determine $\varphi(2T)$ as the relative phase between the two signals, one from a reference cell at zero perturber pressure, the other from the main cell at nonzero perturber pressure.

The detailed calculations of the Appendix show that the probe absorption fringe signal should peak at a time $2T$ relative to the first input pulse. This is confirmed by the experiments and is easily understood. Since the population inversion contains a fringelike velocity dependence, the probe-induced polarization contains a cosinusoidally modulated distribution of Doppler-shifted frequencies. When the velocity integral is performed to find the net time-dependent probe-induced polarization, the result depends on the Fourier transform of $\cos vT$ which peaks in the time domain at time T relative to the second pulse when the grating is formed. As discussed in
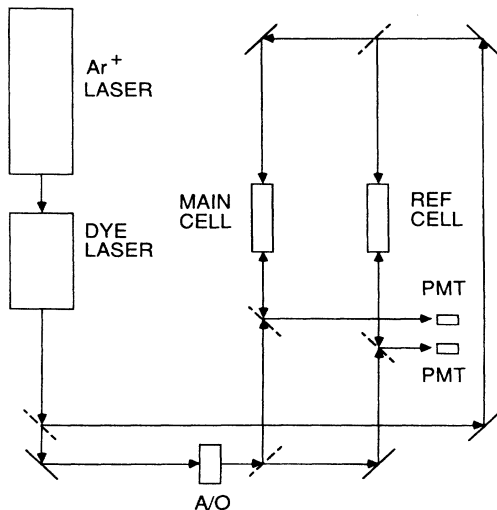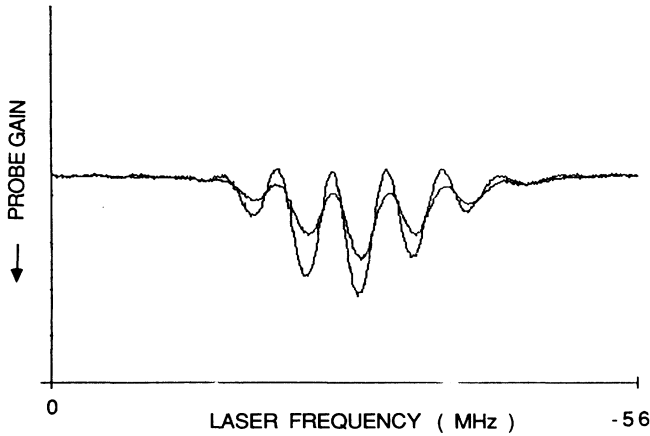
FIG. 1. Experimental scheme.

FIG. 2. Probe absorption vs laser frequency for $T=95$ ns. The larger (smaller) signal corresponds to the reference (main) cell. Laser frequency increases to the left. Note the phase shift between the two signals.

detail in the Appendix, this is closely related to stimulated echo formation.

An important point is that the collision-induced phase $\varphi(2T)$ *does not change* after the time $2T$, when the probe-induced polarization comes into equilibrium and tracks the population inversion. It is for this reason that probe absorption measurements are made at a time just after the peak signal at time $2T$.

As discussed below, $\varphi(2T)$ is a nonlinear function of T from which the imaginary part of the velocity-changing kernel can be obtained by Fourier transformation. In order to determine this function, measurements are done for a number of input pulse separations T and hence observation times $2T$, as shown in Fig. 4.

According to the Appendix, in the presence of collisions, the macroscopic polarization is altered both during the period T between the first two pulses when the inversion fringe is formed, and during the probe polarization build-up period T relative to the second pulse. Both destruction and velocity changes occur, causing nonexponential decay of the amplitude of the fringelike absorption signal, analogous to that measured in echo experiments.[8] In addition, the phase of the probe absorption fringe at time $2T$ is shifted according to

$$\varphi(2T) = -2\operatorname{Im}\int_0^T \Gamma_{ba}(t)dt \ , \tag{2}$$

where

$$\Gamma_{ba}(t) = \gamma_{\text{tot}} - \int_{-\infty}^{\infty} d(\Delta v)W_{ba}(\Delta v)\cos(k\Delta vt) \ . \tag{3}$$

Equation (3) shows that the imaginary part of the one-dimensional collision kernel $W_{ba}(\Delta v)$ is related by Fourier transformation to the phase $\varphi(2T)$. This result uses the same approximations as in the analysis of two-pulse-echo experiments,[4] where the real part of integral given in Eq. (2) is measured. It is assumed in writing Eq. (3) that the kernel is a function only of the velocity change Δv along the laser-pulse propagation direction and is symmetric in Δv. This approximation is valid for

excitation near the center of the Doppler profile for the small-angle velocity changes which the radiator survives, provided that the initial and final velocity changes are small compared to the perturber thermal speed.[14] At small time delays T, the rate $\operatorname{Im}\Gamma_{ba}(T)$ reduces to the usual line shift δ_s.[4] In this case, $\varphi(2T) = -2\delta_s T$, exactly the result one obtains by shifting the resonance frequency ω_0 by δ_s in the time-dependent phase ϕ above. In general, for a given pulse delay, only velocity changes smaller than the period $\sim\lambda/T$ of the population Ramsey fringe can cause phase shifts without degrading the amplitude of the fringelike part of the absorption signal. Hence, the pulse separation controls the velocity resolution. As $T\to\infty$, the slope of the phase versus time-delay curve is determined by the imaginary part of the total collision rate $\operatorname{Im}\gamma_{\text{tot}}$, *independent* of the details of the kernel shape. Hence, in the limit $T\to\infty$

$$\varphi(2T) \to c_0 - 2\operatorname{Im}\gamma_{\text{tot}}T \ , \tag{4}$$

where c_0 is the y intercept of the asymptotic line. The measured value of the y intercept can be related to the value of the imaginary kernel for $\Delta v =0$ using Eqs. (2) and (3) for large T and the representation of the δ function, Eq. (6), below as

$$c_0 = \frac{2\pi}{k}W_{ba}(0) \ . \tag{5}$$

Equation (3) can be inverted to find the kernel in terms of the measured phase versus time-delay curve. For excitation near the center of the Doppler profile, the kernel is a symmetric function of Δv.[14] Using the cosine representation of the δ function valid in the positive quadrant $(T,\Delta v \geq 0)$

$$\delta(b-a) = \frac{2}{\pi}\int_0^{\infty}\cos ub \cos ua \, du, \quad a,b\geq 0 \tag{6}$$

one obtains

$$\operatorname{Im}W_{ba}(\Delta v) = \frac{k}{\pi}\int_0^{\infty} dt \cos(k\Delta vt)$$
$$\times[\operatorname{Im}\gamma_{\text{tot}} - \operatorname{Im}\Gamma_{ba}(t)] \ . \tag{7}$$

This result can be cast in a more practical form by integrating by parts to obtain the imaginary kernel directly in terms of the measured phase versus time-delay data. With Eqs. (2) and (4) the kernel is given by

$$\operatorname{Im}W_{ba}(\Delta v) = \frac{k}{2\pi}\left[c_0 + \int_0^{\infty} dT \, k\Delta v \sin(k\Delta vT) \right.$$
$$\left. \times[\varphi(2T) + 2\gamma_{\text{tot}}T - c_0]\right] \ , \tag{8}$$

where the integration by parts is done in such a way that the integrand $\to 0$ as $T\to\infty$. In this way, the kernel can be obtained from the data as long as the asymptotic region has been measured. This result is closely related to that obtained previously for real kernels.[15]

III. PHASE DETERMINATION BY FAST FOURIER TRANSFORM

As described in Sec. II, the collision-induced phase $\varphi(2T)$ can be determined by comparing the relative phase of the sinusoidal absorption signals obtained from the reference and main cells, Fig. 2. Accurate determination of the phase is achieved by using fast Fourier transformation of the probe absorption traces as shown below.

In the experiments, the laser frequency typically is scanned ~ 56 MHz. For the shortest input pulses (~ 12–15 ns) and time delays, the scan width is increased to ~ 84 MHz to accommodate the larger width of the fringe pattern. The frequency is scanned by means of a computer-generated ramp voltage which controls the length of a Fabry-Pérot cavity to which the laser is locked. The scan is divided into 512 points at each of which two analog-to-digital channels sample the output of two boxcar amplifiers, one for the reference cell, the other for the main cell. At an input pulse repetition rate of 17 kHz, about 100 samples are taken at each laser frequency point in a 5-ms sample time. The total scan time for 512 points is then ~ 2.5 s. The absolute laser frequency is not stabilized since only the *relative* phase is required for the measurements. In order to maintain centering of the absorption traces within the scan range, however, the computer is programmed to shift the start voltage, holding the ramp excursion fixed. In this way, approximate centering of the signals is achieved during the time required to step the pulse separation T through a number of values, taking typically five frequency scans at each value. Pulse timing is accomplished with a computer-controlled-delay generator (SRS DG535) the output of which is sent to a home-built pulse-duration generator. In addition, the delay generator is used to control the boxcar gate timing for observation just after the optimum time $2T$ relative to the first input pulse. As discussed above, the phase does not change after $2T$.

For a typical scan, the fringelike part of the probe absorption trace takes the form

$$F(\Delta;a) = A_c(\Delta - a)\cos[2T(\Delta - a) + \varphi]$$
$$+ A_s(\Delta - a)\sin[2T(\Delta - a) + \varphi] , \qquad (9)$$

where to simplify the notation, we take $\varphi = \varphi(2T)$. Note that as a function of Δ, the fringe "frequency" is just $2T$. The goal of the technique described in this section is to accurately extract the collision-induced phase shift $\varphi(2T)$ of this fringe from the data.

The fringelike absorption traces which are obtained in the experiments are shifted somewhat from the center of the laser frequency scan, which we define here as $\Delta \equiv 0$, and occur at an offset frequency a. It is useful to center the traces with respect to the scan range by numerically shifting the traces by a discrete number of frequency steps. After shifting, the signal is nearly centered and takes the form of Eq. (9) with $a \to a + b$, where b is the frequency shift, and $a + b$ is nearly zero. The resonance at $\Delta = a + b$ then occurs nearly at the center of the scan. The reason for centering the scan will become clear below.

The absorption trace as a function of Δ is Fourier transformed according to

$$F(\tau) = \int_{-\infty}^{\infty} d\Delta\, e^{-i\Delta\tau} F(\Delta; a + b)$$
$$\simeq e^{-i\Phi(\tau)} A(\tau - 2T) , \qquad (10)$$

where τ is the time conjugate to the frequency Δ and

$$A(\tau - 2T) = \tfrac{1}{2}\int_{-\infty}^{\infty} d\Delta'\{ A_c(\Delta')\cos[(\tau - 2T)\Delta']$$
$$- A_s(\Delta')\sin[(\tau - 2T)\Delta']\} \qquad (11)$$

is a real amplitude due to the symmetry and antisymmetry of the coefficients of the cosine and sine terms, respectively, in Eq. (11) as derived in the Appendix. In Eq. (11) terms $\propto \exp i(\tau + 2T)$ are dropped, and we consider $\tau \geq 0$ only. This procedure is valid when the $\tau = 0, \pm 2T$ Fourier transform peaks are well resolved, as is the case for input pulse durations small compared to $2T$. The peak of the Fourier-transform amplitude then determines $2T$. Using Eq. (9) for $F(\Delta; a + b)$ and Eq. (11), the phase of the Fourier transform is given by

$$\Phi(\tau) = \varphi - \tau(a + b) . \qquad (12)$$

Equation (12) shows that if $a + b \neq 0$, the transform phase will vary linearly with τ. By adjusting the shift b so that $a + b \simeq 0$, this τ dependence is nearly eliminated. This reduces the phase error due to imperfect determination of the value of $2T$. It is for this reason that the shift b is adjusted to center the trace within the scan range. Figure 3
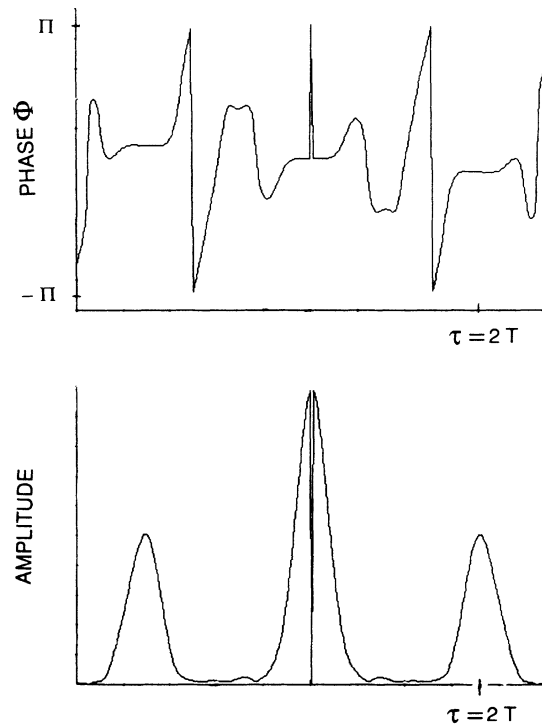

FIG. 3. Amplitude and phase of the Fourier transform of a probe absorption vs laser frequency trace. Note that the phase $\Phi(\tau)$ is nearly horizontal at the amplitude peak for $\tau = 2T$.

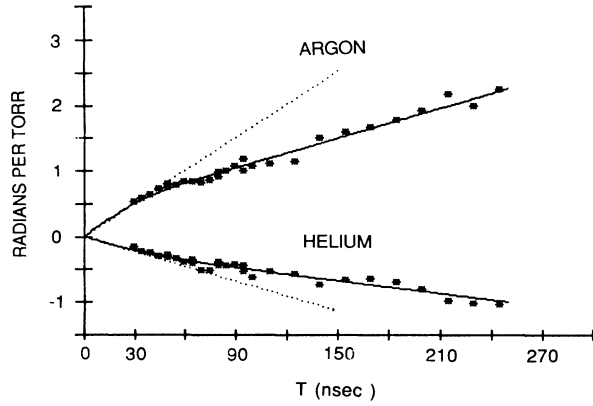FIG. 4. Collision-induced phase $\varphi(2T)$ vs time delay T. The solid curves show the fits obtained using Eq. (18). The dotted lines show the phase $\varphi(2T) = -2\delta_s T$ for the pressure shifts obtained from the Lamb-dip measurements.

shows the magnitude and phase $\Phi(\tau)$ for the Fourier transform of one probe absorption versus laser frequency trace which has been shifted as discussed above. According to Eq. (9) with $a \to a + b$, $\Phi(2T)$ is just the phase of the fringelike absorption trace at the center of the scan $\Delta = 0$. The *relative* phase between the reference and main cell signals, which are *identically* shifted in the analysis, is then given by

$$\varphi(2T;P) = \Phi_{\text{main}}(2T;P) - \Phi_{\text{ref}}(2T) , \qquad (13)$$

where T is the pulse separation and P is the perturber pressure in the main cell.

In actual analysis of the data, the peak of the transform magnitude (for $\tau \neq 0$) is first determined to find the effective value of $2T$. The results are in good agreement with the values expected based on the known scan range and input pulse separation T. Then the phase of the transform for both the reference and main cell signals are determined at the *same* value of $\tau = 2T$. To increase resolution, the 512 data points are loaded into a 4096-point array before taking the transform. Further, the constant background component corresponding to $\tau = 0$ is subtracted off prior to taking the transform so that maximum dynamic range is obtained. By measuring phase versus time curves at a number of different perturber pressures, phase versus pressure is obtained for each pulse separation T. At zero perturber pressure in the main cell, the relative phase typically is quite small, ≤ 0.05 rad with a variation of about 0.01 rad. The relative phase is found to vary quite linearly in perturber pressure. Fitting the phase versus pressure to a straight line gives the phase shift per Torr for each value of T yielding the results shown in Fig. 4.

IV. RESULTS

Time-dependent phase curves for argon and helium perturbers were obtained for a range of time delays between 30 and 245 ns. Data taken for time delays between 60 and 245 ns lie on nearly a straight line with a slope which determines $\text{Im}\gamma_{\text{tot}}$ independently of the details of

the kernel shape as discussed above. The data presented in this paper are not quite good enough to be inverted according to Eq. (8). However, the imaginary kernel width and velocity-changing rate can be estimated from the data which contain substantial information. Since the phase must go through the origin at $T = 0$, the y intercept of the asymptotic line for large T is meaningful and determines the magnitude of the imaginary kernel for zero velocity change according to Eq. (5). This can be used to estimate the kernel width by noting that the integral (i.e., the area) of the kernel for all velocity changes must be the imaginary part of the velocity changing rate $\text{Im}\gamma_v$. It follows from Eq. (3) for short times[4] that

$$\text{Im}\gamma_{\text{tot}} = \delta_s + \text{Im}\gamma_v . \qquad (14)$$

Hence, by determining the pressure shift δ_s, the velocity changing rate $\text{Im}\gamma_v$ and the kernel width can be determined. The pressure shift can be determined both from the slope of the short-time data where $\varphi(2T) \propto -2\delta_s T$ and independently using a Lamb-dip technique as described below.

For simplicity, the imaginary kernel is taken to be given by a Gaussian distribution, so that its width can be compared with that obtained for the real part of the kernel in the Yb system.[8] In this case,

$$\text{Im}W_{ba}(\Delta v) = \text{Im}\gamma_v \frac{e^{-(\Delta v/\delta v)^2}}{\delta v \sqrt{\pi}} . \qquad (15)$$

From Eq. (15), the width is given in terms of the kernel maximum as

$$\delta v = \frac{\text{Im}\gamma_v}{\text{Im}W_{ba}(0)\sqrt{\pi}} = \frac{2\sqrt{\pi}\,\text{Im}\gamma_v}{kc_0} , \qquad (16)$$

where Eq. (5) has been used. By substituting the Gaussian kernel into Eq. (3) the time-dependent decay rate takes the form

$$\text{Im}\Gamma_{ba}(t) = \text{Im}\gamma_{\text{tot}} - \text{Im}\gamma_v e^{-(k\delta vt/2)^2} , \qquad (17)$$

where k is the optical wave vector. Using Eq. (2), the phase can be written as

$$\varphi(2T) = -2\,\text{Im}\gamma_{\text{tot}}T + 2\frac{\text{Im}\gamma_v\sqrt{\pi}}{k\delta v}\text{erf}\left[\frac{k\delta vT}{2}\right]$$

$$= -2\,\text{Im}\gamma_{\text{tot}}T + c_0\text{erf}\left[\frac{k\delta vT}{2}\right] , \qquad (18)$$

where

$$\text{erf}(x) = \frac{2}{\sqrt{\pi}}\int_0^x dy\, e^{-y^2}$$

and $\text{erf}(\infty) \to 1$.

Equation (18) is fit to the data as follows. First, the y intercept c_0 and the total collision rate are determined from the long-time data. Then, the width of the kernel is calculated from Eq. (16) using Eq. (14) to find $\text{Im}\gamma_v$ in terms of an input guess for the pressure shift δ_s. $\varphi(2T)$ is then calculated and compared to the data using a χ^2 fit. The parameters for the best fits (solid curves, Fig. 4) are given in Table I. The pressure shifts were compared with

TABLE I. Imaginary kernel collision parameters.

| Perturber | δ_s (MHz/Torr) | | Imγ_{tot} (MHz/Torr) | Imγ_v (MHz/Torr) | δv (cm/s) |
	Phase versus time-data	Lamp-dip method			
He	+0.58	+0.60	$+0.26(^{+0.04}_{-0.04})$	−0.32	$350(^{+175}_{-120})$
Ar	−1.50	−1.34	$-0.60(^{+0.04}_{-0.05})$	+0.90	$479(^{+122}_{-76})$

those measured using a Lamb-dip technique to obtain Doppler-free resonances in the reference and signal cells. Fifty scans each were taken at 0, 500, and 1000 mTorr perturber pressure. The pressure shifts of the broad lines were obtained by fitting a polynomial to the top of each of the averaged resonances, using the reference cell signal as a marker, and were found to scale quite linearly with pressure. The shifts per Torr obtained by the Lamb-dip method are given in Table I in parentheses (LD) and compare nicely with those obtained from the phase versus time data.

V. CONCLUSIONS

Measured imaginary kernel collision parameters for an Yb two-level optical radiator contrast sharply with the parameters obtained for the real kernel in the same system.[8] In the latter case, the measured velocity changes were diffractive in magnitude, 57 and 123 cm/s for argon and helium, respectively. The larger result for helium in this case is attributed to the smaller range of the helium interaction potentials, leading to a larger diffraction angle. Note that the diffractive velocity is nearly independent of perturber mass.[4,8] By contrast, the width of the imaginary part of the collision kernel for argon is about eight times larger than that of the real part, suggesting that classical angle collisions may be important. In addition, the imaginary kernel width using helium perturbers falls below the argon value. This further supports a classical scattering picture, since the lighter perturber results in a smaller velocity change. However, the diffractive width for helium perturbers is only a few times smaller than the imaginary kernel width, so that the measured velocity change is not really classical.

An interesting feature of the data is the lack of curvature at longer time delays T. Using $k\delta vT/2 = 1$ as a crude estimate of the velocity change resolution [see Eq. (18)], we expect that velocity changes as small as 70 cm/s would be observable for the time scale of the data. This resolution is comparable to the diffractive velocity changes discussed above. Curiously, the phase versus time data appear to be quite linear at the longest time delays, suggesting that the diffractive contribution to the imaginary kernel is small in this system. Experiments at longer time delays would be useful in confirming this behavior.

It is interesting to discuss our data in the framework of the qualitative trajectory "separation" picture of Ref. 4. The line-broadening rates for both helium and argon perturbers are ~5 MHz/Torr, about half of the total collision rate. Since the line-broadening rates are not small, one expects that the average optical phase shift which

occurs during a collision is not small. As pointed out in Ref. 4, when the broadening rate is not small, one expects that for classical velocity changes (i.e., large compared to diffractive), the *difference* between the classical scattering angles for each of the superposed states exceeds the diffraction angle which determines the uncertainty in the classical trajectories. This corresponds to "separation" of the classical trajectories. From our results, the optical radiator therefore appears to survive such collisions.

A possible explanation is that the relative phase of the ground- and excited-state scattering amplitudes does not oscillate rapidly enough to average out the one-dimensional kernel unless the scattering angle is quite large compared to the diffraction angle. In this case, the summation over scattering angles which determines the one-dimensional kernel for the superposition state might not be negligible for the range of velocity changes observed in this experiment. In this case, the qualitative trajectory separation arguments of Ref. 4, which require very different collision potentials and large scattering angles, might not be an accurate enough approximation. Note that in the measurement of the real part of the kernel, the large diffractive velocity-changing cross section due to long-range collisions may have masked a larger angle scattering contribution due to collisions at shorter range and hence smaller cross section. It is also possible that some region of impact parameter exists for which the classical deflections for each of the superposed states are similar, due to the effects of both attractive and repulsive potentials. However, this seems inconsistent with the large broadening rate. Further, for the imaginary kernel to exist, the potentials cannot be too nearly identical, or the phase shift and hence the imaginary kernel will vanish.

Our first attempts at modeling the kernel using quasi-classical scattering amplitudes, based on the stationary phase method and the van der Waals potentials, yield velocity-changing rates which appear to be somewhat small to adequately model the data. However, it is likely that the approximations made in the analysis are too crude. In addition, the imaginary part of the calculated diffractive kernel appears to yield too large a velocity changing rate to be consistent with the data. Further, as stated above, diffractive scattering does not seem to contribute strongly to the phase versus time data obtained in these experiments.

In conclusion, we have demonstrated the measurement of time-dependent collision-induced optical phase in macroscopic coherence, using a simple technique based on velocity-space Ramsey fringes. The nonlinear time dependence of the phase versus time-delay curves ob-

tained using this technique provides important information about the imaginary part of the velocity-changing kernel for an optical radiator (optical coherence). The imaginary kernel is particularly sensitive to large phase-shift collisions, in contrast to the real kernel for which long-range small-phase-shift encounters play a dominant role. From the measurements, it appears that the Yb optical radiator survives much larger velocity changes than previously measured or expected on the basis of qualitative classical trajectory separation arguments. It is likely that more detailed calculations are needed to model the data, which measure velocity changes which are perhaps not sufficiently large in comparison with diffractive velocity changes for classical scattering to be strictly valid.

The absorption fringe technique exploited here to study imaginary collision kernels can be extended to study the phase of the macroscopic coherence created in any type of inhomogeneously broadened medium. This may provide new information about some of the condensed matter systems investigated previously using echo-related techniques.[16]

ACKNOWLEDGMENTS

APPENDIX: PHASE MEASUREMENT BY VELOCITY-SPACE GRATINGS

In the following, we calculate the time-dependent absorption coefficient for a weak c.w. probe wave which propagates in the $-\hat{z}$ direction into a cell which has been previously excited by two pump pulses. The pump pulses, which are separated by a time interval T, propagate in the $+\hat{z}$ direction, and create a fringelike population inversion or grating in the sample as described above. The derivation begins with the density-matrix equations for a two-level atom including a collision-integral term.[1-3] These equations take the form

$$\frac{\partial \rho_{ba}}{\partial t} + v\frac{\partial \rho_{ba}}{\partial z} = -\frac{i}{\hbar}[H^{(0)} + U, \rho]_{ba} + \left[\frac{d\rho_{ba}}{dt}\right]^{coll} ,$$

(A1)

where a, b are either of the two coupled atomic states and the interaction with the laser field is given by

$$U = -\boldsymbol{\mu}\cdot\mathbf{E}(\mathbf{R}, t) .$$

(A2)

The collision term takes the form

$$\left[\frac{d\rho_{ba}}{dt}\right]^{coll} = -\Gamma_{ba}\rho_{ba}(v, z, t)$$
$$+ \int dv' W_{ba}(v - v')\rho_{ba}(v', z, t) .$$

(A3)

It is assumed in writing Eq. (A3) that the one-dimensional collision kernel W_{ba} is a function of the velocity change $\Delta v = v - v'$ only. This is valid for excitation near the center of the Doppler profile $v \simeq 0$ for the small-angle collisions of interest here.[14] Further, for the population equations $b = a$, the effect of spontaneous emission in returning population to the ground state is neglected. The effect of spontaneous emission is to alter the grating *amplitude*, which is not of interest here.

In solving for the collisional evolution, it is convenient to use a Green's-function technique. The Green's function satisfies the following equation:

$$\left[\frac{\partial}{\partial t} + v\frac{\partial}{\partial z}\right]G_{ba}(v, z, t; v', z', t') + \Gamma_{ba}G_{ba}(v, z, t; v', z', t')$$
$$- \int dv'' W_{ba}(v - v'')G_{ba}(v'', z, t; v', z', t') = \delta(v - v')\delta(t - t')\delta(z - z') .$$

(A4)

The Green's function can be determined by Fourier transformation of Eq. (A4) (Ref. 17) and takes the form

$$G_{ba}(v, z, t; v', z', t') = \theta(t - t')\int_{-\infty}^{\infty}\frac{dk'}{2\pi}\int_{-\infty}^{\infty}\frac{|k'|d\tau}{2\pi}e^{ik'[z - z' - v'(t - t')]}e^{ik'(v - v')\tau}\exp\left[-\int_{\tau}^{\tau + t - t'}\Gamma_{ba}(k'\tau')d\tau'\right] .$$

(A5)

The time-dependent decay rate is given by

$$\Gamma_{ba}(k\tau) = \Gamma_{ba} - \int_{-\infty}^{\infty}d\Delta v W_{ba}(\Delta v)\cos(k\Delta v\tau) ,$$

(A6)

with $\Delta v = v - v'$ the one-dimensional velocity change along the laser-field propagation direction, and Γ_{ba} is the total-collision rate for the coherence ρ_{ba} (or the population when $b = a$). This result assumes that the kernel is a symmetric function of Δv, which is valid provided that v and v' are small compared to the perturber speed.

We begin by calculating the probe absorption with the field of the backward propagating probe taking the form

$$\mathbf{E}(\mathbf{R}, t) = \frac{\hat{e}\mathscr{E}_0}{2}e^{-ikz - i\omega t} + c.c.$$

(A7)

The off-diagonal density-matrix elements are transformed according to

$$\rho_{ba} = \sigma_{ba}e^{-i\omega_0 t} ,$$

(A8)

where $\omega_0 = \omega_b - \omega_a$ is the atomic resonance frequency, assuming that b is the excited state and a the ground state. The evolution equation for the probe-induced coherence then is given by

$$\left[\frac{\partial}{\partial t}+v\frac{\partial}{\partial z}\right]\sigma_{ba}=-\frac{i}{\hbar}U_{ba}e^{i\omega_0't}(\sigma_{aa}-\sigma_{bb})+\left[\frac{d\sigma_{ba}}{dt}\right]^{\text{coll}}.$$

(A9)

The collision term in Eq. (A9) is identical in form to that of Eq. (A3) with $\rho\to\sigma$. With the Green's function, Eq. (A5), the solution for σ_{ba} is readily obtained subject to the initial condition $\sigma_{ba}=0$ at $t\to-\infty$:

$$\sigma_{ba}(v,z,t)=\int_{-\infty}^{\infty}dt'\int_{-\infty}^{\infty}dz'\int_{-\infty}^{\infty}dv'G_{ba}(v,z,t;v',z',t')i\frac{\mu_{ba}\cdot\hat{e}\mathcal{E}_0}{2\hbar}e^{-i\Delta_0t'-ikz'}[\sigma_{aa}(v',t')-\sigma_{bb}(v',t')],$$

(A10)

where $\Delta_0=\omega-\omega_0$ is the probe frequency detuning. Note that the population inversion created by the traveling-wave pump pulses is independent of z, so that the z' integration selects out $k'=-k$ in the Green's function, making the k' integral trivial.

The absorbed probe power per unit volume is then given by

$$\frac{dI}{dz}=-\tfrac{1}{2}\text{Re}(\dot{\mathbf{P}}\cdot\mathbf{E}^*),$$

(A11)

where $I=(c/8\pi)\mathcal{E}_0^2$ and

$$\mathbf{E}=\mathcal{E}_0\hat{e}e^{-ikz-i\omega t}$$

is the probe field written in classical form. The probe-induced polarization is given by

$$\mathbf{P}=\text{Re}2\mu_{ab}\int_{-\infty}^{\infty}\rho_{ba}(v,z,t)dv.$$

(A12)

Carrying out the integrations, and defining $\Delta=\omega-\omega_0$ yields the probe absorption coefficient as

$$\frac{1}{I}\frac{dI}{dz}=-\frac{4\pi k|\mu_{ba}\cdot\hat{e}|^2}{\hbar}\text{Re}\int_{-\infty}^{t}dt'e^{i\Delta_0(t-t')}\exp\left[-\int_0^{t-t'}\Gamma_{ba}(-k\tau')d\tau'\right]$$

$$\times\int_{-\infty}^{\infty}dv'e^{ikv'(t-t')}[\sigma_{aa}(v',t')-\sigma_{bb}(v',t')].$$

(A13)

Equation (A13) gives the time-dependent probe absorption for an arbitrary population inversion. We see that if the population inversion is created at time T in the form of a fringelike pattern $\propto\cos(kv'T)$ as is done in the experiments, then the last integral corresponds to the probe-induced polarization having a cosinusoidal frequency distribution. When this distribution is transformed into the time domain, by performing the v' integral, it peaks for $t-t'=T$, i.e., $t'=t-T$. (Note that since $t'\le t$, the additional peak at $t'=t+T$ never occurs.) The minimum t' for which the fringelike inversion exists is T, the time at which the grating in the inversion is created. Hence the absorption signal corresponding to the fringe cannot be observed before $t\simeq2T$. Thus, the fringe signal increases over a time scale of a pulse duration as the observation time approaches $2T$. In general, as long as the observation time is greater than $2T$, the principal contribution to the observed absorption fringe arises from the peak in the integrand at $t'=t-T$. This behavior is closely related to stimulated-echo formation[18] and has been predicted in other contexts.[16] Physically, the continuous probe field can be considered to be an infinite series of δ-function pulses, one for each value of t', each of which generates a stimulated echo at time $t=t'+T$. The bandwidth of the echo is limited by the Doppler width of the grating which is created in the sample. The width is of the order of the inverse pulse width for the velocity selective excitation of interest here. Hence, the echo duration is the order of the pulse duration. This has the consequence that the signal which is observed at time t is due only to the probe field which was present at a time t' within a pulse width of $t'=t-T$. This is the reason for the peak in the integrand at

$t'=t-T$. Further, we see that for measurements at times greater than $2T$, the signal begins to decrease because the population inversion fringe decays—the probe does not interact with the population fringe as soon as it can.

An important consequence of the echolike behavior is that in the integral of $\Gamma_{ba}(-k\tau')$, which determines the collisional evolution of the optical polarization, one can replace $t-t'$ by T, for observation times greater than $2T$ by more than pulse duration. Hence, the effects of collisions on the amplitude and *phase* of the polarization are dependent only on the pump pulse separation T. This approximation is valid provided that the Doppler shifts corresponding to the measured collision-induced velocity changes are small compared to the pulse bandwidth so that $\Gamma_{ba}(k\tau)$ varies little over the time of a pulse duration.[19] The absorption transient which arises from the first pulse alone is readily shown to make a negligible contribution to the signal for observation times more than a few pulse durations after the second pulse, due to Doppler dephasing—the probe absorption comes into equilibrium with the new population inversion. Hence, the important contributions to the absorption signal observed at times greater than $t=2T$ can be calculated with the lower limit of integration in Eq. (A13) replaced by $t_2+\tau_2$, the time at which the second pulse ends (see Fig. 5). As long as the observation time is after $t=2T$ by more than a pulse duration, the peak in the integrand will occur for times t' after the second pulse, and will be contained in the integration region. Hence, the population inversion for times *after* the second pulse is all that needs to be determined. We therefore avoid the complicated general integration of Eq. (A13).
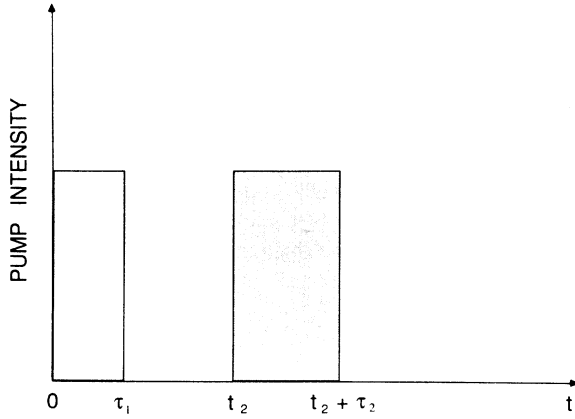
FIG. 5. Pump pulse timing.

To complete the calculation of the probe absorption signal for observation times greater than $2T$, we now find the shape of the population inversion created in the medium by the two forward propagating pump pulses for times just after the second pulse. Figure 5 shows the pulse timing. The calculation is accomplished in two steps. For short pulses, the effect of collisions *during* the pulses is neglected. In this case, the evolution of the system is determined by the interaction with the pump pulses

$$U_p = -\mu \cdot \left[\hat{\mathbf{e}} \frac{\mathscr{E}_p}{2} e^{i(kz - \Omega t)} + \text{c.c.} \right] , \tag{A14}$$

where $\Omega = \omega + \omega_{AO}$ is the acousto-optically shifted laser frequency of the pump pulses. During the time in between and after the pump pulses, the system evolves due to collisions in the absence of the laser fields. It is assumed that the probe field is weak enough that it does not perturb the system. The polarization created by the first pump pulse evolves collisionally during the time interval before the second pulse to alter both the amplitude and the phase of the grating which is created in the population inversion when the second pulse arrives. However, once the inversion fringe is created, Eq. (A13) shows that for observation times $t \geq 2T$, as discussed above, the collision-induced *phase* of the signal remains constant, and the evolution of the probe absorption depends only on the population inversion for times after the second pulse.

With Eq. (A8), the density-matrix equations for times during the pump pulses take the form

$$\frac{\partial \sigma_{ba}}{\partial t} + v \frac{\partial \sigma_{ba}}{\partial z} = \frac{i \mu_{ba} \cdot \hat{\mathbf{e}}}{2\hbar} \mathscr{E}_p(t) e^{ikz - i\Delta_p t} (\sigma_{aa} - \sigma_{bb}) ,$$

$$\frac{\partial (\sigma_{bb} - \sigma_{aa})}{\partial t} = \frac{2i \mu_{ba} \cdot \hat{\mathbf{e}}}{2\hbar} \mathscr{E}_p(t) e^{ikz - i\Delta_p t} \sigma_{ab} + \text{c.c.} ,$$

$$\tag{A15}$$

$$\frac{\partial (\sigma_{bb} + \sigma_{aa})}{\partial t} = 0 ,$$

where the rotating-wave approximation has been used

and $\Delta_p = \Omega - \omega_0$ is the pump frequency detuning. The last equation expresses conservation of population during the pump pulses. This is valid for the short pulses of interest here, during which velocity-changing collisions can be neglected.

In order to solve these equations, it is convenient to make the following substitutions:

$$\beta_p(t) = \frac{\mu_{ba} \cdot \hat{\mathbf{e}}}{\hbar} \mathscr{E}_p(t) ,$$

$$\sigma_{ba} = i(u - iv) e^{ikz - i\Delta_p t} ,$$

$$n = \sigma_{bb} - \sigma_{aa} , \tag{A16}$$

$$\Delta' = \Delta_p - kv .$$

With these substitutions, the evolution equations take the form

$$\dot{u} - i\dot{v} - i\Delta'(u - iv) = -\frac{\beta_p(t)}{2} n ,$$

$$\dot{n} = 2\beta_p(t) u . \tag{A17}$$

By taking the real and imaginary parts of Eqs. (A17), a set of first-order equations for u, v, and n is readily obtained. These are straightforwardly solved by differentiating the u equation with respect to t to obtain

$$\ddot{u} + \beta'^2 u = 0, \quad \dot{v} = -\Delta' u, \quad \dot{n} = 2\beta_p u , \tag{A18}$$

where β_p is the magnitude of the pump Rabi frequency when the pump field is on (square pulses are assumed) and

$$\beta' = (\beta_p^2 + \Delta'^2)^{1/2} . \tag{A19}$$

The u equation is then readily solved, from which v and n are then obtained by integration. It is convenient to work backwards from the second pulse which we take to turn on at time t_2 and to turn off at time $t_2 + \tau_2$. According to Eq. (A13) only the population inversion is needed. Just after the second pulse, the inversion is given as

$$n(t_2 + \tau_2) = n(t_2) \left[\frac{\Delta'^2}{\beta'^2} + \frac{\beta_p^2}{\beta'^2} \cos\phi_2' \right] + \frac{2\beta_p}{\beta'} \sin\phi_2' \, u(t_2)$$

$$+ \frac{2\beta_p \Delta'}{\beta'^2} (1 - \cos\phi_2') v(t_2) , \tag{A20}$$

where the effective pulse area for the ith pulse is defined by

$$\phi_i' = \beta' \tau_i . \tag{A21}$$

Equation (A20) gives the population inversion just after the second pulse in terms of u, v, and n just prior to the second pulse. These quantities are in turn determined by collisional evolution from the state of the system just after the first pulse. Since the collision Green's functions determine the evolution of the matrix elements of σ we write

$$u(t_2) = \frac{1}{2i}[e^{-ikz+i\Delta_p t_2}\sigma_{ba}(t_2) - \text{c.c.}],$$

$$v(t_2) = \frac{1}{2}[e^{-ikz+i\Delta_p t_2}\sigma_{ba}(t_2) + \text{c.c.}], \qquad (A22)$$

$$n(t_2) = \sigma_{bb}(t_2) - \sigma_{aa}(t_2).$$

Then, the matrix elements of σ at time t_2 are given in terms of those at time τ_1, just after the first pulse by

$$\sigma_{ba}(v,z,t_2)$$

$$= \int_{-\infty}^{\infty} dz' \int_{-\infty}^{\infty} dv' G_{ba}(v,z,t_2;v',z',\tau_1)\sigma_{ba}(\tau_1). \quad (A23)$$

This result is readily obtained from Eq. (A9) for $U_{ba}=0$ using the Green's function solution, by adding a source term to the right-hand side of the form

$$\delta(t'-\tau_1)\sigma_{ba}(\tau_1),$$

which creates the correct initial conditions and vanishes for $t' \geq \tau_1$. Similar equations can be written for the population terms σ_{bb}, σ_{aa} with the coherence Green's function replaced by the appropriate population Green's function G_{bb}, etc. Since the populations are independent of z for the problem at hand, the population Green's functions depend only on the velocity v and t. We will not write them here, however, because the population collisional evolution affects only the amplitude and not the phase which is of interest. The population term in Eq. (A20)

$\propto n(t_2)$ does not contain phase information from the first pulse and therefore does not contribute to the fringe in the population inversion. Hence, only the coherence terms $u(t_2)$ and $v(t_2)$ need be calculated in terms of the conditions just after the first pulse. For a pulse which begins at $t=0$ and ends at $t=\tau_1$, Eqs. (A18) are readily solved assuming only $n(0)\neq 0$ to obtain

$$u(\tau_1) = -\frac{\beta_p}{2\beta'}\sin\phi_1' \, n(0),$$

$$v(\tau_1) = \frac{\beta_p \Delta'}{\beta'^2}\frac{1-\cos\phi_1'}{2} n(0), \qquad (A24)$$

$$n(\tau_1) = \left[\frac{\Delta'^2}{\beta'^2} + \frac{\beta_p^2}{\beta'^2}\cos\phi_1'\right]n(0).$$

Hence, with the definition of σ_{ba} in terms of u and v above,

$$\sigma_{ba}(\tau_1) = i[u(\tau_1) - iv(\tau_1)]e^{ikz-i\Delta_p \tau_1},$$

$$\qquad (A25)$$

$$\sigma_{ba}(\tau_1) = \left[\frac{\beta_p \Delta'}{\beta'^2}\frac{1-\cos\phi_1'}{2} - i\frac{\beta_p}{2\beta'}\sin\phi_1'\right]e^{ikz-i\Delta_p \tau_1}n(0).$$

Using Eq. (A23) with the Green's function Eqs. (A5), the z' integration yields a δ function that selects out $k'=k$, rendering the k' integration trivial. The following result is then obtained for the coherence at time t_2:

$$\sigma_{ba}(v,z,t_2) = \int_{-\infty}^{\infty} \frac{k\,d\tau}{2\pi} \int_{-\infty}^{\infty} dv' e^{-ikv'(t_2-\tau_1)} e^{ik(v-v')\tau} \exp\left[-\int_{\tau}^{\tau+t_2-\tau_1}\Gamma_{ba}(k\tau')d\tau'\right]$$

$$\times \left[\frac{\beta_p \Delta'}{\beta'^2}\frac{1-\cos\phi_1'}{2} - i\frac{\beta_p}{2\beta'}\sin\phi_1'\right]n(0,v')e^{ikz-i\Delta_p \tau_1}. \qquad (A26)$$

Equation (A26) can be integrated using the same approximations employed for the two-pulse photon echo.[4] If short pulses are used for the excitation (i.e., a large Rabi frequency β_p), then the velocity spread of the polarization created by the first pulse will be large compared to the collisional small-angle velocity changes which are of interest here. In this case, if the v' integration were performed first, the resulting function of $(t_2 - \tau_1 + \tau)$ which appears in the integrand will be sharply peaked at $\tau = -(t_2 - \tau_1)$ compared to the time scale over which

$\Gamma_{ba}(k\tau)$ varies. Hence, the exponential collision factor can be taken outside of the integrals and evaluted with $\tau = -(t_2 - \tau_1)$. With the collision factor removed, Eq. (A26) is most straightforwardly evaluated by performing the τ integral first with the substitution $\bar{\tau} = \tau + t_2 - \tau_1$. This permits the removal of a factor $\exp[-ikv(t_2-\tau_1)]$ from the integral so that all terms in the integrand are broad functions of v'. The $\bar{\tau}$ integration then yields a δ function which selects $v = v'$, rendering the v' integral trivial. The result for the coherence is then given by

$$\sigma_{ba}(v,z,t_2) = e^{ikz-i\Delta_p t_2}\exp\left[-\int_0^{t_2-\tau_1}\Gamma_{ba}(-k\tau')d\tau'\right]e^{i\Delta'(t_2-\tau_1)}\left[\frac{\beta_p \Delta'}{\beta'^2}\frac{1-\cos\phi_1'}{2} - i\frac{\beta_p}{2\beta'}\sin\phi_1'\right]n(0,v). \qquad (A27)$$

With this result, the u and v terms in Eq. (A20) for $n(t_2+\tau_2)$ are easily evaluated using Eq. (A22). If we choose for our observation a time shortly after the peak signal at $t \simeq 2t_2$ we can neglect the population evolution due to collisions after the time $t_2 + \tau_2$, since the signal arises only due to the probe wave which interacts with the population fringe as soon as it is formed, at $t' \simeq t_2 + \tau_2 \simeq T$, as discussed above. In this case, we expect a peak in the integrand of Eq. (A13) at $t' \simeq t_2 + \tau_2$ when the results for $n(t_2+\tau_2)$ are used. This turns out to be the case only for the σ_{ba} terms of Eq. (A22). The complex conjugate terms $\propto \sigma_{ab}$ peak outside of the integration range, after the time t. Using these ideas, the fringelike part of the absorption coefficient can be written as

$$\left[\frac{1}{I}\frac{dI}{dz}\right]_{\text{fringe}} = -\frac{4\pi|\mu_{ba}\cdot\hat{\mathbf{e}}|^2}{\hbar}\text{Re}\int_{t_2+\tau_2}^{t}dt'e^{i\Delta_0(t-t')}\exp\left[-\int_0^{t-t'}\Gamma_{ba}(-k\tau')d\tau'\right]$$

$$\times\exp\left[-\int_0^{t_2-\tau_1}\Gamma_{ba}(-k\tau')d\tau'\right]$$

$$\times\int_{-\infty}^{\infty}dv\,e^{ikv(t-t')+i\Delta'(t_2-\tau_1)}\left[\frac{\beta_p\Delta'}{\beta'^2}\frac{1-\cos\phi_1'}{2}-i\frac{\beta_p}{2\beta'}\sin\phi_1'\right]$$

$$\times\left[\frac{\beta_p\Delta'}{\beta'^2}\frac{1-\cos\phi_2'}{2}-i\frac{\beta_p}{2\beta'}\sin\phi_2'\right]2\sigma_{aa}(0,v)\,,\qquad\text{(A28)}$$

where the lower integration limit is taken as $t_2+\tau_2$ according to the echo analogy discussed above and

$$n(0,v)=-\sigma_{aa}(0,v)=-\frac{N_0}{u\sqrt{\pi}}e^{-v^2/u^2}\,,\qquad\text{(A29)}$$

with u the thermal speed. Using the same argument as that of Eq. (A27), the amplitude of the integrand in Eq. (A28) is seen to be a broad function of v relative to the scale of collision-induced velocity changes of interest here. If the v integral is done first then, noting that $\Delta'=\Delta_p-kv$, the resulting function of $t-t'-(t_2-\tau_1)$ will be sharply peaked at $t-t'=t_2-\tau_1$ relative to the time scale over which $\Gamma_{ba}(k\tau)$ varies appreciably. Hence, the collision term can be factored outside the integral and evaluated with $t-t'=t_2-\tau_1$. With this factor removed, the integral in Eq. (A28) takes the form

$$\int_{-\infty}^{\infty}dv\int_{t_2+\tau_2}^{t}dt'e^{i\Delta_0(t-t')}e^{i\Delta_p(t_2-\tau_1)}$$

$$\times e^{ikv[t-t'-(t_2-\tau_1)]}f(v)\,,$$

where $f(v)$ is the broad function of v in the integrand and the order of integration for v and t has been interchanged. To obtain the detuning dependence of the probe signal, it is convenient to make the substitution $\tilde{t}=t-t'-(t_2-\tau_1)$. This yields the form

$$e^{i(\Delta_0+\Delta_p)(t_2-\tau_1)}\int_{-\infty}^{\infty}dv\int_{-(t_2-\tau_1)}^{t-2t_2-\tau_2+\tau_1}d\tilde{t}\,e^{i(kv+\Delta_0)\tilde{t}}f(v)\,.$$

If the observation time is taken to be later than that of the signal peak, at $t=2[t_2+(\tau_2-\tau_1)/2]$ by the order of a few pulse widths, the $\tilde{t}$ integral yields approximately a δ function which selects $kv=-\Delta_0$ in the integrand, when the velocity integral is done. This determines the shape of the envelope of the fringelike part of the probe signal. Putting this all together we obtain finally

$$\left[\frac{1}{I}\frac{dI}{dz}\right]_{\text{fringe}}$$

$$=\alpha_0e^{-\Delta_0^2/(ku)^2}$$

$$\times\exp\left[-2\,\text{Re}\int_0^{t_2-\tau_1}\Gamma_{ba}(-k\tau')d\tau'\right]g(\Delta)\,,\quad\text{(A30)}$$

where the Doppler-broadened absorption coefficient is

$$\alpha_0=\frac{4\pi|\mu_{ba}\cdot\hat{\mathbf{e}}|^2}{\hbar ku/\sqrt{\pi}}N_0\qquad\text{(A31)}$$

and the line-shape function is given by

$$g(\Delta)=A_c(\Delta)\cos[2\Delta(t_2-\tau_1)-2\phi_{ba}]$$

$$+A_s(\Delta)\sin[2\Delta(t_2-\tau_1)-2\phi_{ba}]\,,\qquad\text{(A32)}$$

where $2\Delta\equiv\Delta_0+\Delta_p$, so that $\Delta=\omega-\omega_0+\omega_{AO}/2$ is identical to the detuning of Eq. (1) of Sec. II. The effective time separation T between the square input pulses is $T=t_2-\tau_1$. This equals zero when the square pulses coalesce into one long pulse as it should.

The phase ϕ_{ba} is given by

$$\phi_{ba}=\text{Im}\int_0^{t_2-\tau_1}d\tau'\Gamma_{ba}(-k\tau')\,,\qquad\text{(A33)}$$

so that with Eq. (A6) for $\Gamma_{ba}(-k\tau)$, and $t_2-\tau_1=T$, $\varphi(2T)=-2\phi_{ba}(T)$ reproduces Eq. (2) as it should. The amplitudes in Eq. (A32) are given by

$$A_c(\Delta)=\frac{4\beta_p^2}{\beta'^2}\sin\frac{\phi_1'}{2}\sin\frac{\phi_2'}{2}$$

$$\times\left[\cos\frac{\phi_1'}{2}\cos\frac{\phi_2'}{2}-\left(\frac{2\Delta}{\beta'}\right)^2\sin\frac{\phi_1'}{2}\sin\frac{\phi_2'}{2}\right]\,,$$

$$A_s(\Delta)=-\frac{4\beta_p^2}{\beta'^2}\sin\frac{\phi_1'}{2}\sin\frac{\phi_2'}{2}\frac{2\Delta}{\beta'}\sin\left[\frac{\phi_1'+\phi_2'}{2}\right]\qquad\text{(A34)}$$

and are symmetric and antisymmetric functions of Δ, respectively. The pulse areas $\phi_i'=\beta'\tau_i$ are given by Eq. (A21) where β' is of the same form as Eq. (A19) with Δ' evaluated at $kv=-\Delta_0$, the probe detuning, so that

$$\beta'=(\beta_p^2+4\Delta^2)^{1/2}\,,\qquad\text{(A35)}$$

where $\Delta=\omega-\omega_0+\omega_{AO}/2$. These results substantiate the statements made in the text concerning the fringelike part of the absorption signal which is of primary interest in this paper.

In real experiments, the input pulses are not square, but smoothly vary. In this case, the actual input pulse time separation T should be the time delay between the peaks of the pulses. This correctly determines the measured fringe "frequencies" and properly corresponds to the period of collisional evolution between the input pulses and between the second input pulse and the signal measurement time.

For completeness, we include a calculation of the background signal which is present in addition to the fringelike absorption. This is necessary for comparison of the

calculated and experimental absorption line shapes. In order to simplify the calculations, we neglect collisions and spontaneous emission and determine the maximum signal. The probe absorption is again given by Eq. (A13), but we take $\Gamma_{ba}(-k\tau)$ equal to zero. As above, for observation times more than a few pulse widths after the second input pulse, the effect of the first pulse alone is unimportant—the probe absorption comes into equilibrium with the new population inversion. Hence, the lower limit of integration in Eq. (A13) can be set equal to $t_2+\tau_2$ as above. The background absorption arises from the non-fringe-like part of the population inversion for times after the second pulse. This is due to the $n(t_2)$ term which was neglected in Eq. (A20) in calculating the fringelike part of the absorption. Using Eq. (A24) the relevant part of the population inversion is given by

$$n(t_2+\tau_2,v)_B = \left[\frac{\Delta'^2}{\beta'^2}+\frac{\beta_p^2}{\beta'^2}\cos\phi_1'\right]$$

$$\times \left[\frac{\Delta'^2}{\beta'^2}+\frac{\beta_p^2}{\beta'^2}\cos\phi_2'\right] n(0,v) , \quad (A36)$$

FIG. 6. Calculated probe absorption vs laser frequency detuning Δ. $T=t_2-\tau_1=75$ ns, $\tau_1=\tau_2=25$ ns, and pulse areas $\beta_p\tau_1=0.55$ rad. Note that the separation between the centers of the input pulses is 100 ns.

where the subscript B denotes background and all quantities are as in Eq. (A16), etc. With Eqs. (A16) and (A29) the background absorption is given by

$$\left[\frac{1}{I}\frac{dI}{dz}\right]_B = -\alpha_0\frac{1}{\pi}\text{Re}\int_{t_2+\tau_2}^t dt'e^{i\Delta_0(t-t')}\int_{-\infty}^\infty k\,dv\,e^{ikv(t-t')}\left[\frac{\Delta'^2}{\beta'^2}+\frac{\beta_p^2}{\beta'^2}\cos\phi_1'\right]\left[\frac{\Delta'^2}{\beta'^2}+\frac{\beta_p^2}{\beta'^2}\cos\phi_2'\right]e^{-v^2/u^2} .$$

$$(A37)$$

Now, the velocity integral in Eq. (A37) is just the Fourier transform of a broad function of kv, the Doppler bandwidth being the order of an inverse pulse duration for the velocity selective excitation of interest here. Hence, the integral over v yields a sharply peaked function of $t-t'$ so that the principal contribution to the signal arises from the region where $t'\simeq t$. Thus, the region of t' integration includes the peak, as expected from the echo analogy discussed above with $T=0$. The integration is most readily accomplished by evaluating the t' integral first. This takes the form

$$\frac{1}{\pi}\text{Re}\int_0^{t-t_2-\tau_2}d\bar{t}\,e^{i(\Delta_0+kv)\bar{t}} , \quad (A38)$$

where the substitution $\bar{t}=t-t'$ has been made and the rest of the integrand in Eq. (A37) is real. Writing the real part of the exponential factor as a cosine and making the change of variables $\bar{t}\to-\bar{t}$ in the complex conjugate term which results yields for Eq. (A38) the result $\delta(kv+\Delta_0)$ for observation times more than a pulse width after the second pulse. The final result for the background term is
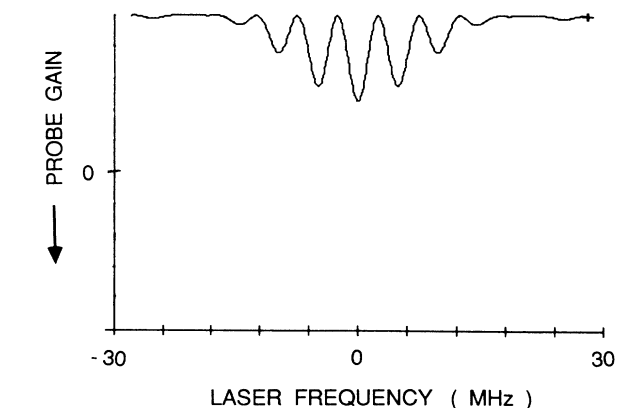
obtained by performing the velocity integral which selects out $kv=-\Delta_0$ to give

$$\left[\frac{1}{I}\frac{dI}{dz}\right]_B = -\alpha_0 e^{-\Delta_0^2/(ku)^2}\left[\frac{4\Delta^2}{\beta'^2}+\frac{\beta_p^2}{\beta'^2}\cos\phi_1'\right]$$

$$\times \left[\frac{4\Delta^2}{\beta'^2}+\frac{\beta_p^2}{\beta'^2}\cos\phi_2'\right] , \quad (A39)$$

where β' in Eq. (A35) and the Δ are defined as above. When collisions are included, it is easy to show that the condition that $t-t'\simeq0$ in the integrand of Eq. (A37) causes the background term to undergo an ordinary pressure shift $\delta_s=\text{Im}\Gamma_{ba}(0)$ (Ref. 4) provided that the pressure broadening $\gamma_{ab}=\Gamma_{ba}(0)$ is small compared to the Doppler bandwidth of the excitation pulses. With these results, the expected signal in the absence of decay, including both the background and fringelike absorption, Eqs. (A39) and (A30), is plotted in Fig. 6. The shape nicely reproduces the experimentally observed fringe profiles.

[1]E. W. Smith, J. Cooper, W. R. Chappell, and T. Dillon, J. Quant. Spectrosc. Radiat. Transfer **11**, 1547 (1971); **11**, 1567 (1971).

[2]P. R. Berman, Phys. Rev A **5**, 927 (1972).

[3]See V. A. Alekseev, T. L. Andreeva, and I. I. Sobelman, Zh. Eksp. Teor. Fiz. **62**, 614 (1972) [Sov. Phys.—JETP **35**, 325 (1972)], and references therein.

[4]For a recent review, see P. R. Berman, T. W. Mossberg, and S. R. Hartmann, Phys. Rev. A **25**, 2550 (1982).

[5]J. Schmidt, P. R. Berman, and R. G. Brewer, Phys. Rev. Lett. **31**, 1103 (1973).

[6]See, R. L. Shoemaker, Annu. Rev. Phys. Chem. **30**, 239 (1979), and references therein.

[7]R. Kachru, T. J. Chen, S. R. Hartmann, T. W. Mossberg, and

P. R. Berman, Phys. Rev. Lett. **47**, 902 (1981).

[8]R. A. Forber, L. Spinelli, J. E. Thomas, and M. S. Feld, Phys. Rev. Lett. **50**, 331 (1983).

[9]See, for example, S. N. Bagaev, E. V. Baklanov, and V. P. Chebotaev, Pis'ma Zh. Eksp. Teor. Fiz. **16**, 344 (1972) [JETP Lett. **16**, 243 (1972)].

[10]J. E. Thomas, P. Laverty, and K. Stokes, Bull. Am. Phys. Soc. **33**, 1011 (1988).

[11]P. J. Laverty, K. D. Stokes, and J. E. Thomas, Phys. Rev. Lett. **62**, 1611 (1989).

[12]Ye. V. Baklanov, B. Ya. Dubetsky, and V. P. Chebotaev, Appl. Phys. **9**, 171 (1976); Ye. V. Baklanov, V. P. Chebotaev, and B. Ya. Dubetsky *ibid.* **11**, 201 (1976); J. C. Bergquist, S. A. Lee, and J. L. Hall, Phys. Rev. Lett. **38**, 159 (1977); M. M. Salour and C. Cohen-Tannoudji, *ibid.* **38**, 757 (1977); R. Teets, J. Eckstein, and T. W. Hansch, *ibid.* **38**, 760 (1977).

[13]E. Buhr and J. Mlynek, Phys. Rev. Lett. **57**, 1300 (1986); see E. Buhr and J. Mlynek, Phys. Rev. A **36**, 2684 (1987), and

references therein.

[14]For a discussion of this point, see J. M. Liang, L. A. Spinelli, R. W. Quinn, R. R. Dasari, M. S. Feld, and J. E. Thomas, Phys. Rev. Lett. **55**, 2684 (1985); J. E. Thomas, A. P. Ghosh, and M. A. Attili, Phys. Rev. A **33**, 3029 (1986); J.-L. Gouet and P. R. Berman, *ibid.* **17**, 52 (1978); P. R. Berman, T. W. Mossberg, and S. R. Hartmann, *ibid.* **25**, 2550 (1982).

[15]S. M. Cameron, Ph.D. thesis, M.I.T., 1986.

[16]M. Mitsunaga and R. G. Brewer, Phys. Rev. A **32**, 1605 (1985); A. Schenzle, R. G. Devoe, and R. G. Brewer, *ibid.* **30**, 1866 (1984).

[17]V. P. Kochanov, S. G. Rautian, and A. M. Shalagin, Zh. Eksp. Teor. Fiz. **72**, 1358 (1977) [Sov. Phys.—JETP **45**, 714 (1977)].

[18]T. Mossberg, A. Flushberg, R. Kachru, and S. R. Hartmann, Phys. Rev. Lett. **42**, 1665 (1979).
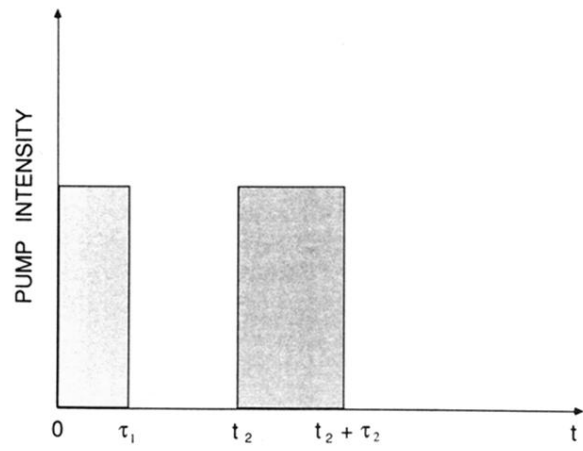
[19]See, for example, P. R. Berman, J. M. Levy, and R. G. Brewer, Phys. Rev. A **11**, 1668 (1975).

FIG. 5. Pump pulse timing.